THE APPLICATION OF NUCLEAR REACTIONS FOR QUANTITATIVE HYDROGEN ANALYSIS IN A VARIETY OF DIFFERENT MATERIALS PROBLEMS

G. J. Clark*, C. W. White, D. D. Allred† and B. R. Appleton
Solid State Division, Oak Ridge National Laboratory**
Oak Ridge, Tennessee 37830

F. B. Koch
Bell Laboratories
Murray Hill, New Jersey 07974

and

C. W. Magee
RCA Laboratories
Princeton, New Jersey 08540

ABSTRACT

The application of nuclear reaction techniques to hydrogen analysis problems in metallurgical, mineralogical and semi-conductor areas are described. Hydrogen analyses and profiles obtained with both the $^{1}H(^{19}F,\alpha\gamma)^{16}O$ and $^{1}H(^{15}N,\alpha\gamma)^{12}C$ reactions are presented. The advantages and disadvantages of the two techniques are discussed. Both crystalline and amorphous materials are examined. Particular emphasis will be given to interpretive problems associated with analyzing the data. Various corrections to the data will be discussed, including off-resonance cross-section corrections and lower energy resonance corrections. The hydrogen content of electrodeposited hard gold films has been determined as a function of plating conditions. Hydrogen contents as high as 9 atom % have been measured. The hydrogen profile of natural and synthetic SiO_2 samples was determined. Hydrogen was found to be quite stable in amorphous silica samples but highly mobile in crystalline quartz samples under the analysis conditions. A hydrogen depth profile for a film of

---

*Guest scientist from Minerals Research Labs., C.S.I.R.O., North Ryde, Australia.

†NSF Energy-Related Postdoctoral Fellow.

**Operated by Union Carbide Corp. under contract with the ERDA.

glow and discharge deposited amorphous silicon (~ 4500 Å thick) has been obtained and will be compared with a profile measured by secondary ion mass spectrometry (SIMS) on the same sample.

1. INTRODUCTION

It is important to understand the role hydrogen plays in energy related materials [1] as many physical properties of solids are modified by the presence of hydrogen. In many cases, quantitative information is required on the depth distribution of hydrogen in a material, as well as its total hydrogen content. Many of the conventional techniques of elemental analysis such as ESCA, Auger, XRF, neutron or charged particle activation, Rutherford backscattering, and electron microprobe are not directly applicable to hydrogen determination. The application of nuclear reactions has the potential of providing quantitative depth information on the total hydrogen content of materials. It has been shown [2] that many different nuclear techniques can be used for hydrogen depth profiling. In this paper we describe the application of two of these nuclear reactions for hydrogen analysis in materials problems associated with metallurgical, mineralogical and semiconductor research areas. For our measurements we used the strong, narrow, isolated resonances in the cross sections of the $^{1}H(^{19}F,\alpha\gamma)^{16}O$ and the $^{1}H(^{15}N,\alpha\gamma)^{12}C$ nuclear reactions.

The following sections of this paper discuss the experimental apparatus, the advantages and disadvantages of each of these reactions, the problems in data analysis related to lower energy resonances and finite off-resonance cross section values. We will conclude with examples of hydrogen profiling measurements in the important problem areas indicated above.

2. TECHNIQUE

Only a brief description of the measurement technique will be given here, as it has been well described elsewhere [2,3,4].

The reaction $^{1}H(^{19}F,\alpha\gamma)$ exhibits a strong resonance at 16.44 MeV in the laboratory system with a peak cross section of 0.5 barn and a width of about 90 keV producing 6.1, 6.9 and 7.1 MeV γ-rays from the de-excitation of the residual excited ^{16}O nucleus [5]. Thus if a material containing hydrogen is irradiated with ^{19}F ions at an energy slightly greater than the resonance energy, the ^{19}F ions will be slowed down until at a certain depth, X_R, the resonance energy will be reached and the resonance reaction will occur producing γ-rays of the appropriate energy. The yield of γ-rays will be proportional to the local hydrogen concentration in a thin layer ΔX_R at the depth X_R. At greater depths the ^{19}F energy will be below the resonance energy. The depth X_R at which the resonance occurs is determined by the stopping power dE/dX for ^{19}F ions in the sample under analysis while the thickness ΔX_R being analyzed is determined by the width of the resonance and energy straggling in the ^{19}F beam. Measuring the γ-ray yield as a function of the ^{19}F beam energy thus gives a direct indication of the hydrogen concentration as a function of depth in the sample.

The depth X_R is related to the incident beam energy E_i by the relation:

$$E_i - X_R \left(\frac{dE}{dX}\right)_{\frac{E_R + E_i}{2}} = E_R. \qquad (1)$$

where E_R is the resonance energy and $\frac{dE}{dx}$ is the stopping power. Stopping power data in this work is taken from Northcliffe and Schilling [6]. For the ^{19}F beam energies of interest here, the dE/dx values are independent of energy to within 3%, which allows the use of a single value for $\frac{dE}{dx}$. Although it is the experience of this group that these stopping powers are too small by $\sim$ 5%, they are the best readily available. Uncertainties in the material density may also contribute to uncertainties in the depth x_R.

The depth resolution Δx_R that can be obtained with the ^{19}F beam depends on the resonance width, Γ, and the energy straggling of the beam, Δx_R. The depth resolution Δx_R may be defined as

$$\Delta x_R = \frac{[\Gamma^2 + (\Delta E_R)^2]^{1/2}}{2\left|\frac{dE}{dx}\right|} \tag{2}$$

where, following Bohr [7]

$$\Delta x_R = 2.36\ (4\pi e^4 z^2 Z N x)^{1/2} \tag{3}$$

where e is the electron charge, z and Z the atomic numbers of the projectile and target respectively, and N is the number of target atoms per unit volume. Thus the depth resolution is depth dependent. Typically, the depth resolution for the ^{19}F reaction varies from $\sim$ 250 Å at the surface to 300 Å at a 4000 Å depth in silicon.

For elements of $Z \leq 5$ a ^{19}F ion beam of 16.0 MeV has sufficient energy to overcome the Coulomb barrier and consequently allows nuclear reactions to occur. Care must be taken to ascertain that γ-rays from other possible reactions are not interfering with the γ-rays from the $^{1}H(^{19}F,\alpha\gamma)^{16}O$ reaction.

A second resonance at 17.56 MeV laboratory energy limits the range of utilization of the 16.44 MeV resonance to ∿ 4000 Å in silicon. This problem can partially be avoided by using the same $^{1}H(^{19}F,\alpha\gamma)^{16}O$ reaction to excite a resonance at 6.42 MeV beam energy. This resonance, which has a width of ∿ 45 keV and a peak cross section of 100 millibarns, allows depths up to 1.2 μm in silicon to be probed prior to the onset of another resonance. The use of this reaction at a lower energy also minimizes the possibility of interference from γ-ray production in reactions between ^{19}F and other light elements.

The reaction $^{1}H(^{15}N,\alpha\gamma)^{12}C$ exhibits a strong resonance at 6.39 MeV in the laboratory system with a peak cross section of 200 millibarns and a width of approximately 15 keV, producing 4.43 MeV γ-rays from the de-excitation of the residual excited ^{12}C nucleus [8]. This reaction was used in a manner similar to the ^{19}F reaction to profile the hydrogen content of samples. The depth resolution of the ^{15}N reaction varies from 60 Å at the surface to 200 Å at 4000 Å depth in silicon.

Advantages of the 16.4 MeV ^{19}F beam over the 6.4 MeV ^{15}N beam for hydrogen analysis include:

1) Higher yield for a given integrated beam charge because of the greater resonance cross section and width. For our experimental arrangement the yield is a factor of 13 times greater for the ^{19}F beam than for the ^{15}N beam, all other factors being constant.

2) Lower rate of introduction of damage into the region of sample being examined and a lower value for the total damage introduced into a sample while obtaining a profile. This can be important when hydrogen is mobile under beam conditions.

3) Higher energy γ-rays which have a relatively smaller underlying background in the γ-ray energy spectrum. This allows data to be recorded using higher beam currents.

4) The fact that ^{19}F is an easier beam to obtain from a tandem accelerator.

Advantages of the ^{15}N beam for hydrogen analysis include:

1) Smaller off-resonance cross section simplifying analysis.

2) Superior depth resolution.

3) A large energy or,equivalently,depth range, prior to the onset of the next resonance. In silicas depths to 3.5 μm can be profiled without the need to invoke unfolding techniques.

4) A negligible probability of exciting γ-rays from other light elements.

These advantages in the use of a 6.4 MeV ^{16}N beam also apply, but to a lesser extent, in the use of 6.42 MeV ^{19}F beam resonance.

3. EXPERIMENTAL PROCEDURE

The experimental apparatus for the nuclear reaction measurements is shown in Fig. 1. The $^{19}F^{+3}$ or $^{15}N^{+2}$ beams, provided by the Oak Ridge National Laboratory Tandem Van de Graaff accelerator were collimated to a beam spot of ∿ 0.4 cm dia. striking the target at normal incidence. Beam currents of 30 nA and 10 nA were used for the ^{19}F and ^{15}N beams, respectively. The beam currents were monitored by (1) particles backscattered from a tantalum flipper rotating in the beam, the flipper being calibrated with a Faraday cup and (2) current integrated off the target. The target holder was surrounded by a LN_2 shroud held at -300 volts to suppress electrons from the target. The vacuum in the target chamber was ∿ 10^{-7} Torr. The γ-rays were detected in both a 3" x 3" NaI detector placed approximately 2 cm from the target and at 90° to the target and a 6" x 4" NaI detector placed approximately 10 cm from the target and at 135° to the target.

The hydrogen content of samples studied was determined in absolute terms by comparison of γ-ray yields with similar yields obtained from

calibration samples. The calibration samples used in this work were polyethelyne $[(CH_2)_n]$, Lexan $[(C_{16}H_{14}O_3)_n]$, and a H^+ (10 keV, 4×10^{16} cm^{-2}) implanted silicon wafer. The calibration constants for the ^{15}N and ^{19}F reactions obtained from these different standards had standard deviations of 13% for both beams.

The use of calibration standards in preference to the use of known cross section data [5,8] avoids systematic errors arising from uncertainties in the absolute cross section data, in the experimental geometry, and in the scintillation detector response functions and efficiencies. However, relative cross sections are still required for unfolding the profiles.

Figure 2 shows a profile obtained from the H^+ implanted Si wafer calibration sample. The profile shows a surface layer of hydrogen ($\sim 2 \times 10^{16}$ cm^{-2}) as well as a broad peak centered at 16.72 MeV or, equivalently, 1420 Å ± 200 Å. The measured width of the surface peak was approximately 95 keV, which agrees with the known resonance width. This implies that the surface hydrogen contamination layer is less than 200 Å thick. All samples studied showed a similar large surface peak. To remove this surface hydrogen, a vacuum of the order of 10^{-10} Torr would be required. It would also be necessary to sputter clean the samples *in situ*.

4. DATA ANALYSIS

Interpretive procedures discussed in this section will be oriented towards analyses made with a ^{19}F beam rather than a ^{15}N beam as the former is the more complicated case. Land et al. [9] have discussed general unfolding techniques for the determination of distribution profiles from resonance reaction gamma-ray yields. They assume the resonance shape to be an attenuated Breit-Wigner form. Consequently, the finite off-resonance cross sections and low energy resonances in the cross sections are not treated. Such

contributions are important and must be corrected for in data analysis. It is useful to consider thick and thin samples when discussing these contributions. A thin film is considered to be one in which the energy loss in the film is not great enough to allow the low energy resonances to contribute to the γ-ray yield when the incident beam is above the resonance energy 16.44 MeV. For gold such a film is $\leq$ 5000 Å.

In a thin hydrogen containing film, although the contribution of the low energy resonances to the above threshold γ-ray yield is negligible, the finite off-resonance cross section values can still introduce large contributions to the γ-ray yield because of the hydrogen surface contribution inevitably present. The off-resonance cross section for the ^{19}F reaction at a beam energy in the range 16.1 to 17.4 MeV is typically 1-3% of the maximum cross section value at 16.44 MeV. Therefore, if a film with hydrogen only at the surface is irradiated with ^{19}F ions at any energy above threshold (say 17.25 MeV), the characteristic gamma ray spectrum will be produced by (17.25 MeV) ions interacting with the surface contamination. A more detailed analysis shows that the amount of surface contamination on all the films which were examined was in the range $1\text{-}3 \times 10^{16}$ H atoms/cm^2. In a sample with 10 at. % bulk hydrogen and a surface hydrogen contamination of 2×10^{16}/cm^2, the surface hydrogen contributes only 4% of the γ yield at 17.25 MeV beam energy. Of course, the surface contribution is more significant if the bulk concentration is lower (at 0.4 at. %, the bulk and surface contributions are equal). Unless a film has a wildly varying hydrogen concentration the off-resonance contribution from hydrogen in the bulk of the material is negligible.

In a thick, hydrogen containing, sample the incident beam will lose sufficient energy to permit the low energy resonant reactions to contribute to the γ-ray yield. These low energy resonances will produce γ-rays down to several microns in the sample (~ 2 μm for Au samples). For an infinitely thick sample of high hydrogen concentration the ratio of the yield from a 17.25 MeV ^{19}F beam to that from a 16.1 MeV ^{19}F beam is 4.0, i.e. in a thick, sample of uniform hydrogen concentration one quarter of the yield may be due to low energy resonances. This number is derived from experimental measurements on polyethelene and Lexan. The off-resonance surface contamination problems discussed for a thin film also apply to the thick sample case.

If a hydrogen profile is determined using a 6.4 MeV ^{15}N beam or a 6.4 MeV ^{19}F beam, the corrections must still be made for the off-resonance contribution due to surface contamination. There is no contribution to the γ-ray yield from low energy resonances.

To aid in the interpretation of the yield data as a function of incident beam energy in terms of a hydrogen concentration profile the following procedure was invoked. The depth distribution of hydrogen in the sample, including the surface contamination, was modeled as a histogram. This is illustrated for a specific case in Fig. 3. The depth scale was broken up into segments d_o, d_1, $d_2 \ldots d_j, \ldots d_m$ where d_j denotes the distance from the sample surface to the back side of the histogram segment j and where d_m is then the sample thickness. Each histogram segment j was assigned a hydrogen concentration h_j. The γ-ray yield $Y(E_i)$ for each incident beam energy E_i may then be written

$$Y(E_i) = \sum_{j=1}^{m} a_{ij} h_j \qquad (4)$$

where

$$a_{ij} = k \int_{E_i - d_{j-1} \cdot \frac{dE}{dX}}^{E_i - d_j \cdot \frac{dE}{dX}} \sigma(E)dE \qquad (5)$$

In the above equations k is a calibration constant determined by the experimental arrangement, $\sigma(E)$ is the differential cross section for the nuclear reaction and $\frac{dE}{dX}$ is the stopping power. The determination of k has been discussed in Section 3. Above 15.45 MeV the cross section data, $\sigma(E)$, used in evaluating a_{ij} was taken from the data of Maurel et al.[10] Below 15.45 MeV we used integrated cross sections estimated from measurements on thick polyethelene and Lexan targets. The stopping power data[6] used was estimated iteratively for a mean energy between E_i and E_j where E_j is the energy of the beam at a depth d_j.

The set of simultaneous equations (4) can be solved for h_j if $i \geq m$. The simplest practical case is for a sample containing a uniform hydrogen concentration, h_2, in the bulk and a hydrogen surface contamination h_1. In this case Eq. (4) can be solved as follows for h_1 and h_2 using yield measurements at two energies E_1 and E_2.

$$\begin{aligned} h_1 &= [Y(E_1)\ a_{22} - Y(E_2)\ a_{12}]/D \\ h_2 &= -[Y(E_1)\ a_{21} - Y(E_2)\ a_{11}]/D \end{aligned} \qquad (6)$$

where $D = a_{11}a_{22} - a_{21}a_{12}$.

In practice E_1 and E_2 are energies chosen to be just below and above the resonance respectively. In this simple case, we chose to use for the ^{19}F analyzing beam E_1 = 16.1 MeV and E_2 = 17.25 MeV.

In the subsequent section specific examples of technological interest will be described to illustrate how these data handling procedures can be manipulated to give quantitative hydrogen concentration data for the specific problem at hand.

5. EXAMPLES OF HYDROGEN PROFILING

a. Hydrogen Incorporation in Electrodeposited Hard Gold

Electrodeposited hard gold is strikingly different in structure and properties from bulk pure gold or even electrodeposited pure gold. This makes the material one of considerable technological importance, specifically for sliding electrical contacts. The structure and property differences include an increase in microhardness by factors of 3-4 and gold, normally the most ductile of metals, becomes so brittle that mechanical fabrication is precluded. The grain size of hard gold is of the order of a few hundreths of a micron versus microns or tens of microns in most plated metals. The impurity levels of light elements have been reported to be extraordinarily high. A recent study by Raub [11] reported concentrations of 8-10% atomic % H, 3 atomic % C, 2 atomic % N, 0.5 atomic % O and 1 atomic % of the hardening agent, either Co or Ni.

To clarify the role of hydrogen in hard gold, we have used the $^{1}H(^{19}F,\alpha\gamma)^{16}O$ nuclear reaction to depth profile the concentration of hydrogen in samples representative of the deposits extensively used for sliding electrical contacts. Some of the samples were plated with a bath chemistry containing cobalt ions (Autotronux CI) while other samples were plated with a simpler bath chemistry where the necessary microhardness was obtained by lowering the bath temperature.

A typical profile is shown in Fig. 4. This is for a thick target and consequently corrections had to be made for contributions to the raw yield data from low energy resonances and surface contamination. At each incident energy shown in Fig. 4, a hydrogen concentration was assigned using Eq. (4) with i = 13. Since the hydrogen content in the bulk of the gold is fairly constant an average value for this concentration together with the average hydrogen content of the surface peak could have been obtained using yields

measured at only two energies, say 16.1 and 17.25 MeV, and the two parameter forms of Eq. (4) given in Eq. (6). Using both the multi-parameter and the two parameter approaches, the hydrogen content for a series of samples prepared under different conditions was determined. The results are shown in Table 1. The results establish conclusively that hard gold electro-deposits contain surprising amounts of hydrogen (up to 9 atomic % in the case of CI gold plated samples) and 0-3% in samples produced in cobalt-free bath chemistry. Profiles measured indicated that the hydrogen is uniformly distributed throughout the film. Repeats of the measurement after thermal annealing at 250°C for one hour in air indicated that the hydrogen is trapped in the samples. Mercury dissolution experiments indicated that the hydrogen is present in the samples in a chemically combined form and not as free hydrogen.

b. Hydrogen Incorporation in Quartz and Silica

Griggs and Blacic [12] demonstrated that the introduction of small amounts of water into the quartz structure has a profound influence on the mechanical properties of this material. Under certain conditions the mechanical strength of quartz may be reduced by an order of magnitude. Subsequent work has shown that the OH content influences the mechanisms of glide and climb of dislocations involved in the deformation process. There is also evidence [13] that OH has a similar effect on the dislocations of other silicates. These observations clearly have important implications in the study of tectonic processes. All of the work mentioned has relied upon infrared absorption spectroscopy for the determination of the OH content of quartz. However, infrared determinations may not be of high

accuracy, chiefly because it is difficult to allow for changes in the molar extinction coefficient with band frequency in complex OH spectra.

Tsong et al. [14] used IBSCA (Ion Beam Spectrochemical Analyser) to determine the hydrogen content of a number of silicates. The results show values which are one to two orders of magnitude above those determined by infrared adsorption for similar samples. There is, of course, the possibility that hydrogen may be present in other than OH form.

In view of the important implications associated with high hydrogen contents in quartz, we have used the $^{1}H(^{19}F,\alpha\gamma)^{16}O$ reaction to provide an estimate of (1) the average hydrogen content of a wide range of silicas, and (2) the depth distribution of hydrogen in several of these samples. Both natural and synthetic quartzes were examined. Prior to examination all samples were coated with a graphite film 12 μg cm^{-2} thick to avoid charge build up.

Figure 5 shows the γ-ray yield as a function of beam energy (and depth) in a X_o quartz sample. The profile exhibits three distinct features. They are (1) the hydrogen surface contamination region, (2) a broad region below the surface of approximate thickness 2000 Å where the γ-ray yield is high and (3) a region deep in the crystal where the γ-ray yield is low. (This yield is partially due to off-resonance nuclear reactions occurring with hydrogen in the surface and near-surface regions.) These three regions were seen in all quartz samples examined.

Using a three-parameter version of Eq. (4), we have assigned hydrogen concentrations to the near-surface region and to the bulk region. The results are given in Table II. The hydrogen content of the surface layer was determined also and found to be always in the range $1\text{-}2 \times 10^{16}$ atom cm^{-2}.

A source of uncertainty not included in the results arises from hydrogen mobility under beam bombardment in crystalline quartz samples. The yield of γ-rays as a function of integrated beam charge is shown in Fig. 6 for a range of amorphous and crystalline samples. For the fused silica samples (vitreosil and suprasil) there was no evidence for hydrogen mobility. The quartz and opal samples shows evidence of hydrogen mobility in that the γ-ray yield dropped as a function of integrated charge. The decrease in yield indicated mobility out of the beam path; there was no evidence for mobility into the beam path. This effect implies that the hydrogen values measured are lower limits for crystalline samples. Data, such as shown in Fig. 6, indicated that the results may in fact be up to 50% low. No such uncertainty is to be associated with the results quoted for the fused silica samples. The diffusion process is probably driven by an electric field in the crystal resulting from the electric charge deposited in the crystal by the ^{19}F beam. This could be checked by damaging samples with a neutron flux prior to analysis. We anticipate that the hydrogen preferentially diffuses along the C axis. It was surprising, however, to see no hydrogen mobility in the fused silica samples, vitreosil and suprasil, as sodium mobility in amorphous SiO_2 films under irradiation has been observed [16].

Despite these uncertainties repeated measurements indicated that the general form of the profile seen in Fig. 5 is correct, i.e., the profile consists of a region just below the surface of high concentration and a region in the bulk of the material with a much lower concentration.

The hydrogen concentrations in the bulk region of the samples listed in Table II are much lower than those quoted by Tsong et al. [14] using the ISBCA technique. To within the quoted errors the results are, however, in agreement with the IR data [13,14]. The ^{19}F technique

is not sensitive enough to discern whether there is hydrogen in the sample in excess to that bonded as SiOH and seen in the IR spectra. The hydrogen concentrations quoted for the surface region in Table II are much higher than those found using IR techniques and in better agreement with those quoted by Tsong et al. although there is still considerable scatter between the results. These results imply that Tsong et al. observed such high concentrations because only the surface of the samples was examined while the IR measurements were averaged through the whole sample. There are also possible systematic errors in the IBSCA results due to water vapor in the vacuum system and hydrogen in the ion beam. The beam was not analyzed.

In summary, the nuclear reaction technique used in this study provides a plausible explanation for the substantial disagreement between the IR and IBSCA results for hydrogen in quartz samples. In addition, it illustrates the complex hydrogen profile that exists in quartz. Unfortunately the results, for crystalline samples, have some uncertainty attached to them due to the high mobility of hydrogen in quartz under ion beam bombardment.

c. Hydrogen Incorporated in Amorphous Silicon

The hydrogen content and distribution in glow discharge deposited amorphous silicon films is a technological problem of considerable current interest [17], especially in its relation to the production of cheap solar cells. It is thought that hydrogen which has been incorporated into amorphous silicon films prepared by glow discharge in a silane atmosphere plays an important role in allowing the films to be substitutionally doped.

We have applied two techniques to the quantitative determination of the hydrogen profile in amorphous silicon. The techniques are (1) the independent use of the $^{1}H(^{19}F,\alpha\gamma)^{16}O$ and the $^{1}H(^{15}N,\alpha\gamma)^{12}C$ nuclear reactions and (2) secondary

ion mass spectrometry (SIMS). The measurements were performed on the same film to provide a direct comparison of all the techniques. The amorphous silicon film (a-Si) used in this work was prepared by DC cathodic deposition in silane onto a stainless steel substrate. The gas pressure was 2 Torr, the current density 1 ma cm^{-2} and the substrate temperature 350°C.

The SIMS measurements were performed in a vacuum with a base pressure of 10^{-10} Torr using a finely focussed Ar^+ ion beam for sputtering. At higher pressures deposition of hydrogen containing molecules on the surface represents a constant source of hydrogen to the sample during analysis and makes determination of hydrogen in the bulk of the material extremely difficult. The H^- sputtered species was used for analysis purposes. The technique was calibrated using a H^+ (10 keV, 4×10^{16} cm^{-2}) implanted Si wafer that had, prior to implantation, been heavily damaged with a Si beam.

The hydrogen profile of the a-Si sample as determined by both the $^1H(^{15}N,\alpha\gamma)$ and the $^1H(^{19}F,\alpha\gamma)$ reactions is shown in Fig. 7. The errors shown include both statistical and calibration errors. The sample is thin,so corrections were required only for the off-resonance surface contribution. Also shown in Fig. 7 is the SIMS profile from the same a-Si film. The large yield of H^+ from the surface in the SIMS data is believed to result from surface contamination containing hydrogen. This is completely removed by sputtering to a depth of $\sim$300 Å. The hydrogen concentration in the bulk of the film as determined by the three techniques is $\sim$ $4.3 \times 10^{21}/cm^3$ or 9.0% atomic H,ignoring the front and back surfaces. The absolute magnitude and the profile of hydrogen determined by the two resonance nuclear reactions are in excellent agreement with each other and with the SIMS results. The fact that excellent agreement is obtained shows that in the SIMS measurements there is no significant difference in the hydrogen containing molecular fragments sputtered from the amorphous silicon

film as compared to the ion implanted calibration sample. Also,the chemical environment of the two samples are similar enough that there is no significant difference attributable to matrix chemical effects or differences in sputtered ion neutralization probabilities. These results show that, if proper attention is paid to calibration procedures and the vacuum environment, SIMS can be used for quantitative hydrogen profile measurements in materials such as amorphous silicon.

Infrared measurements on a-Si material prepared in the manner described above have also given hydrogen concentration results similar to our results indicating that the majority of the hydrogen contained in the film is bonded, presumably compensating dangling Si bonds. It should be noted that, in a-Si solar cell development studies,information on the hydrogen profile is a useful diagnostic. Cell failure can frequently be related to interface problems caused by hydrogen build up. Moreover, diffusion of hydrogen at temperatures $\geq$ 350°C can create dangling bonds that degrade cell efficiency.

6. SUMMARY

This work illustrates that the $^{1}H(^{19}F,\alpha\gamma)^{16}O$ and the $^{1}H(^{15}N,\alpha\gamma)^{12}C$ nuclear reactions can be used for hydrogen analysis and depth profiling in a wide range of technological problems. During data reduction,corrections must be made for possible low energy resonance and surface contamination contributions to the total γ-ray yield. Care must also be taken to monitor possible hydrogen mobility. Data handling procedures should be tailored to the specific problem at hand.

The possibility of using SIMS for quantitative hydrogen depth profiling has also been demonstrated.

REFERENCES

1. F. L. Vook, H. K. Birnbaum, T. H. Blewitt, W. L. Brown, J. W. Corbett, J. H. Crawford, A. N. Goland, G. L. Kulcinski, M. T. Robinson, D. N. Seidman, and F. W. Young, Rev. Mod. Phys. 47, Suppl. No. 3(1975).
2. J. F. Zeigler et al. Third International Conference on Ion Beam Analysis, June 27 - July 1, 1977, Washington, D.C.
3. D. J. Leich and T. A. Tombrello, Nucl. Instr. and Meth. 108, 67 (1973).
4. W. A. Lanford, H. P. Trautvetter, J. F. Ziegler, and J. Keller, Appl. Phys. Letters 28 (1976) 566.
5. F. Ajzenberg-Selove, Nuclear Physics A 190 (1972) 1.
6. L. C. Northcliffe and R. F. Schilling, Nuclear Data Tables A7 (1970) 233.
7. N. Bohr, Kgl. Dan. Viden. Selsk., Mat. Fys. Medd. 18 (1948) 8.
8. F. Ajzenberg-Selove, Nuclear Physics A166 (1971) 1.
9. D. J. Land, D. G. Simons, J. G. Brennan and M. D. Brown, Ion Beam Surface Layer Analysis, Ed. G. Meyer, G. Linker, and F. Käppeler, (Plenum Press, New York, 1976) p. 851.
10. B. Maurel, D. Dieumegard and G. Amsel, Catania Working Data, 1974, p. 71-N.
11. C. J. Raub, A. Knodler and J. Lendvay, Plating 63, 35 (1976).
12. D. T. Griggs and J. D. Blacic, Science 147 (1965) 292.
13. D. T. Griggs, Geophys. J. R. Astron. Soc. 14, (1967) 19.
14. I. S. T. Tsong, A. C. McLaren and B. E. Hobbs, Am. Mineral. 61 (1976) 921.
15. W. C. Goobeer and R. W. T. Wilkins, Am. Mineral (1977) in press.
16. D. V. McCaughan, R. A. Kushner (1974) in Characterization of Solid Surfaces, ed. by Philip F. Kane and Graydon B. Larrabee, Plenum Press, New York.
17. D. E. Carlson, IEEE Transaction on Electron Devices ED-24, No. 4, 449 (1977).

FIGURE CAPTIONS

Fig. 1 Schematic representation of the experimental arrangement for the nuclear reaction measurements described in the text.

Fig. 2 Hydrogen profile of H^+ implanted Si wafer.

Fig. 3 Typical histogram used to model , for analysis purposes, the hydrogen profile in a sample.

Fig. 4 Hydrogen depth profile in CI gold plated sample.

Fig. 5 Gamma ray yield as a function of ^{19}F incident beam energy for X_o quartz.

Fig. 6 Gamma ray yield as a function of integrated beam charge for a range of amorphous silica and crystalline quartz samples.

Fig. 7 Hydrogen profiles determined by SIMS and two nuclear reactions in amorphous silicon sample.

TABLE CAPTIONS

Table 1. Summary of plating conditions and hydrogen content of hard gold films.

Table 2. Average hydrogen concentrations in quartz and silica samples for both near surface and bulk regions. Results are compared to IBSCA and IR data on some samples.

Table I. Hydrogen in Hard Gold [H Concentration (Atom %)]

Sample Plating Conditions	Hydrogen Content at. %
Pure Hard Gold--	
10°C Dep.	2.50
20°C Dep.	1.45
30°C Dep.	2.88
45°C Dep.	1.15
70°C Dep.	0.26
CI Type Gold--	
2500 RPM pH = 4.0	6.11
400 RPM pH = 4.0	9.16

Table 2. Hydrogen in Quartz and Silica [H Concentration (Atom %)]

Sample	Near Surface Region (0 to 0.2 μm)	Bulk Region (0.2 μm to 4 μm)	IBSCA [14]	IR [13,14]
Bell (S)	9.7 ± 1.4	0 ± 0.06	----	----
X_o (S)	2.0 ± 0.3	0.16 ± 0.10	13.8	0.9 (0.2)*
W_2 (S)	1.0 ± 0.2	0.97 ± 0.60	7.81	0.15
W_4 (S)	1.3 ± 0.2	0.52 ± 0.30	3.6 to 10.8	0.084
Smoky (N)	5.0 ± 0.7	0.67 ± 0.19	3.6	----
Quartzite (N)	12.0 ± 1.6	7.4 ± 2.0	2.4 to 8.4	----
Toyo (S)	0.5 ± 0.2	0.38 ± 0.30	1.8	----
Blue Opal (N)	10.0 ± 1.5	11.9 ± 2.1	----	----
White Opal (N)	11.3 ± 1.6	9.6 ± 2.2	----	----
Supralsil (S)	3.5 ± 0.5	0.2 ± 0.1	10.2	----
Vitreosil (S)	3.7 ± 0.6	0.1 ± 0.06	6.0	----

S denotes synthetic sample.

N denotes natural sample.

*Recent determination by thermal technique [15].

ORNL-DWG 77-7062

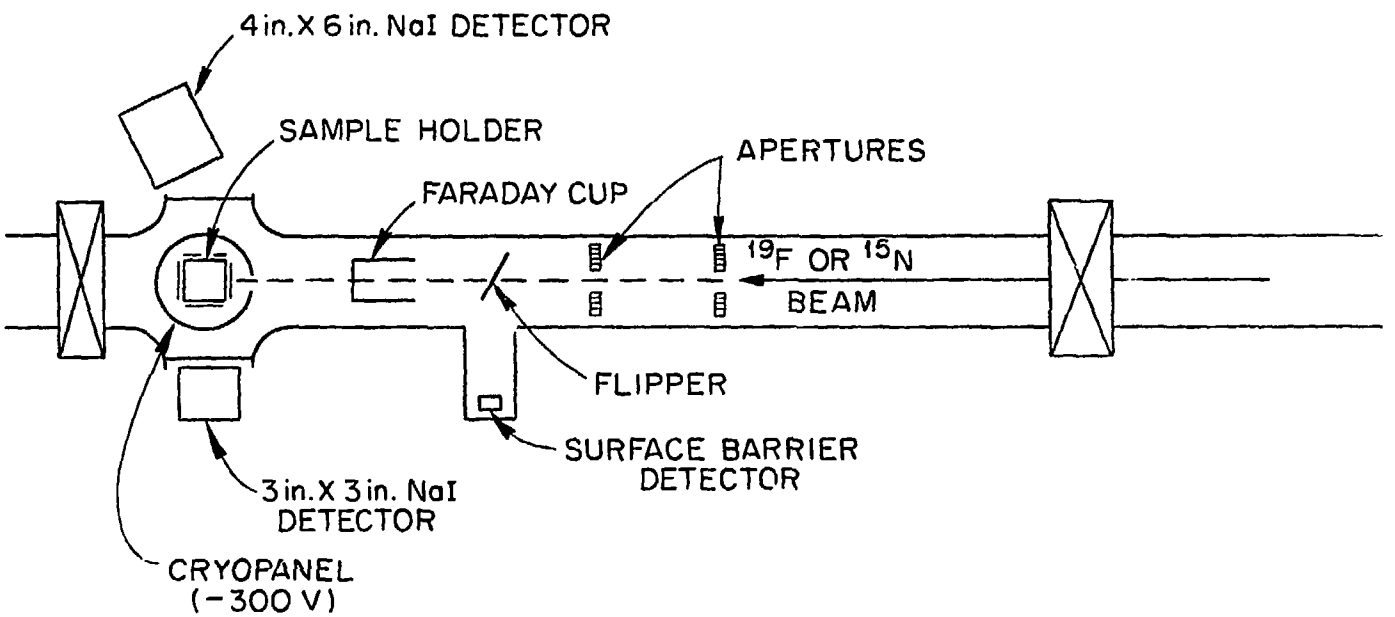

Experimental Apparatus for Hydrogen Depth Profiling.

Fig. 1

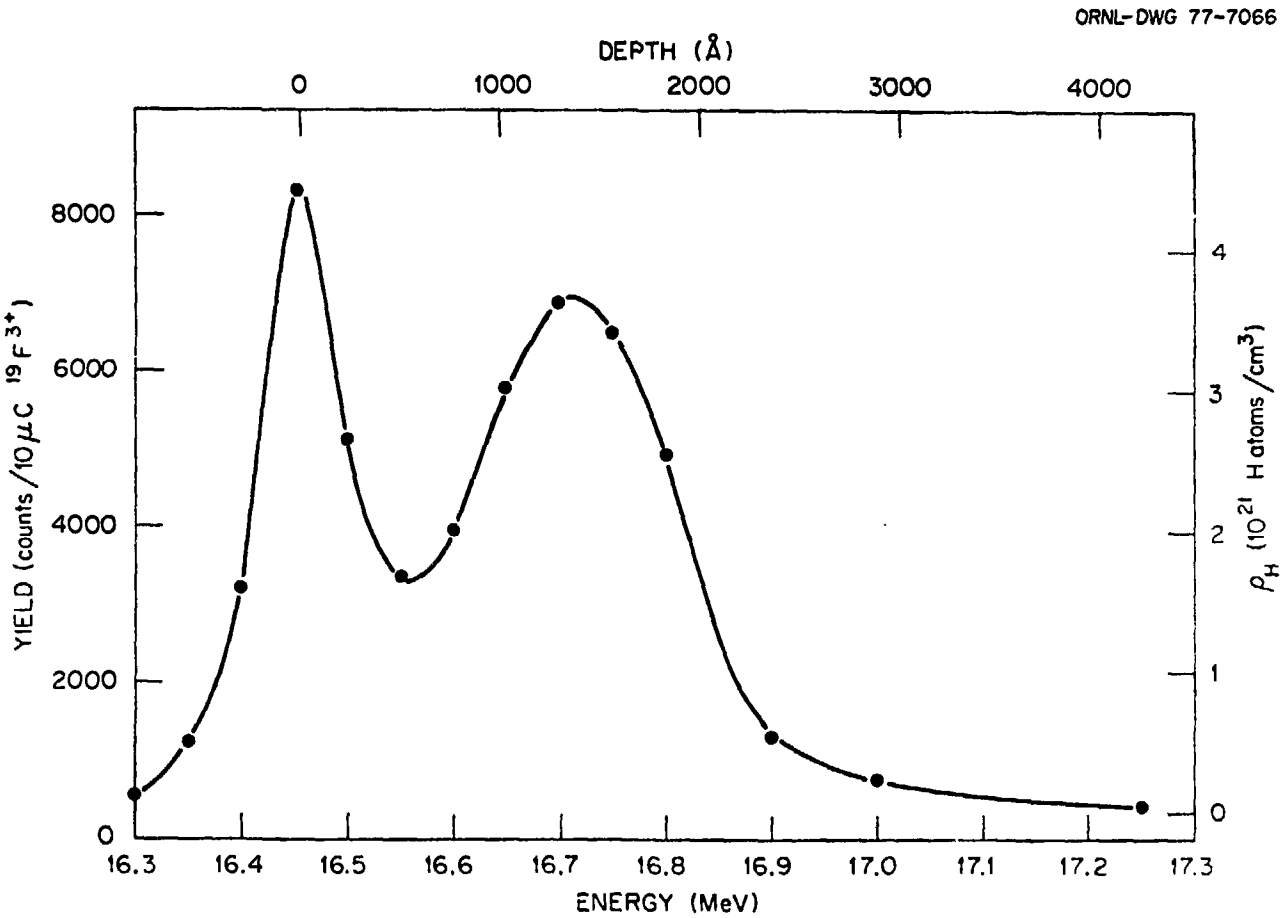

H^+ (10 keV, $4 \times 10^{16}/cm^2$) in Si.

Fig. 2

ORNL-DWG 77-11668

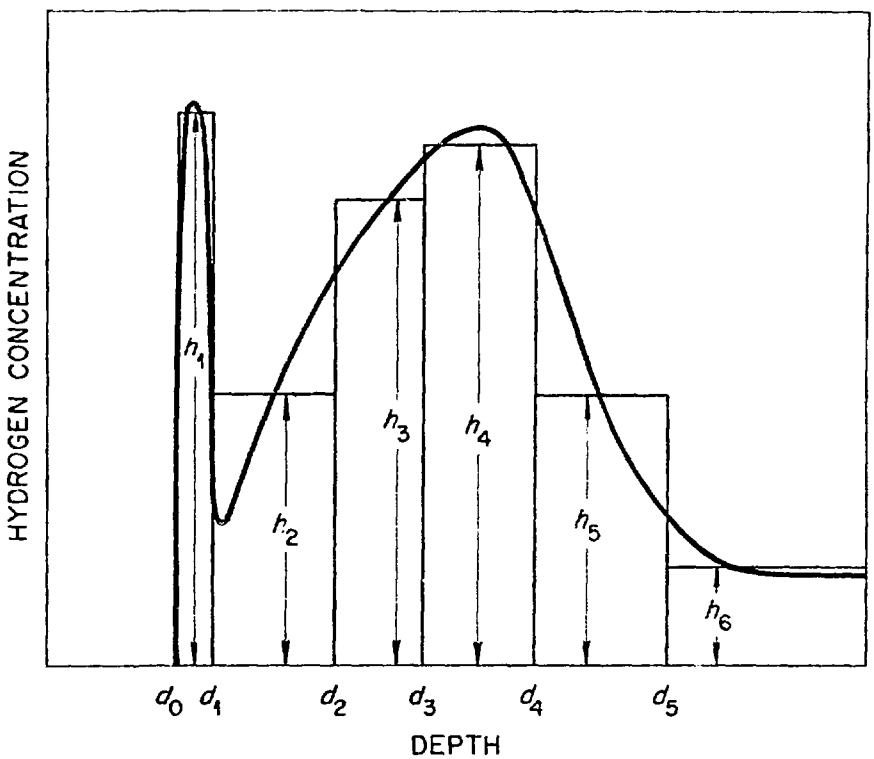

$$Y(E_i) = \sum_{j=1}^{m} a_{ij}\, h_j,\ i = 1, m$$

$$\text{WHERE } a_{ij} = k \int_{\epsilon_1}^{\epsilon_2} \sigma(E)dE$$

$$\text{AND } \epsilon_1 = E_i - d_{j-1}\, dE/dx$$

$$\epsilon_2 = E_i - d_j\, dE/dx$$

Fig. 3

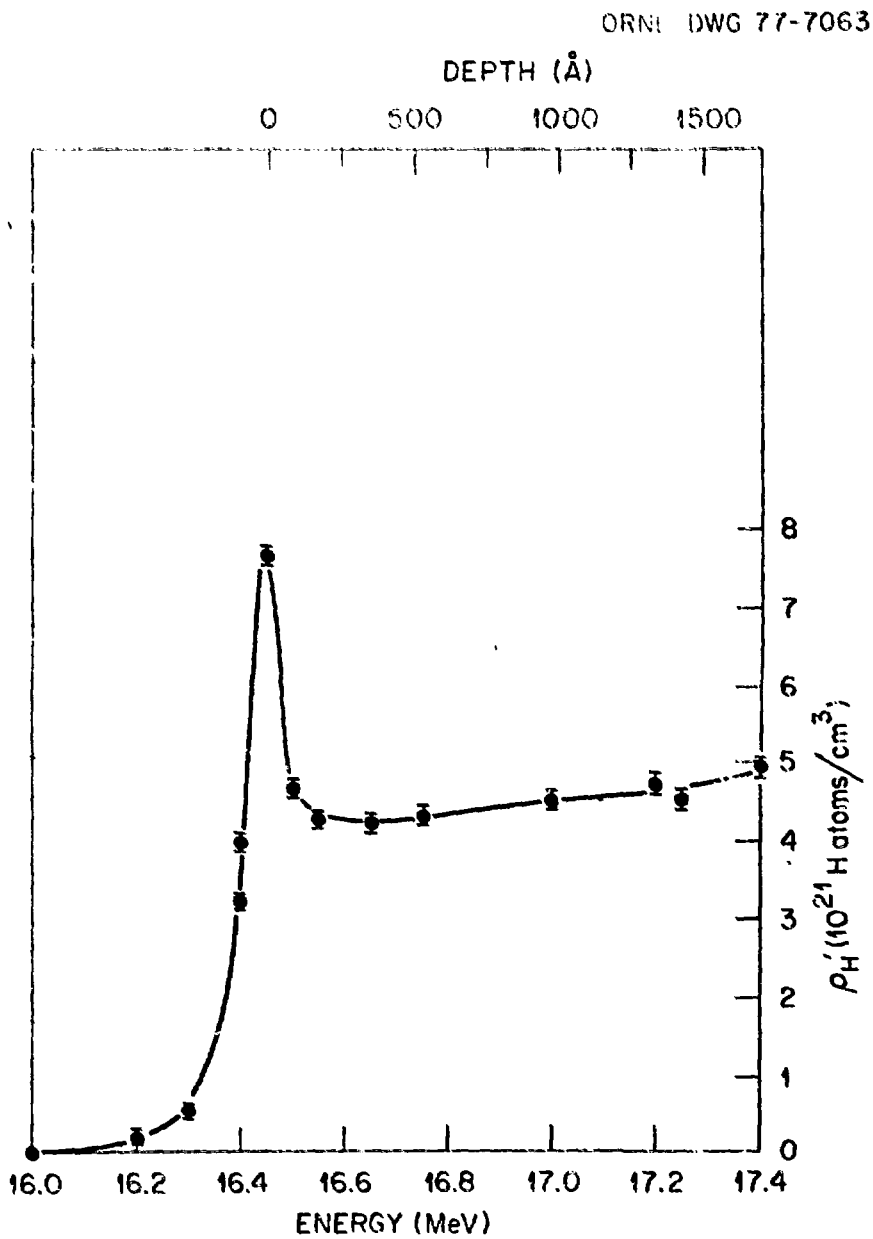

H in CI Hard Au

pH = 4.4

Fig. 4

ORNL-DWG 77-7841R

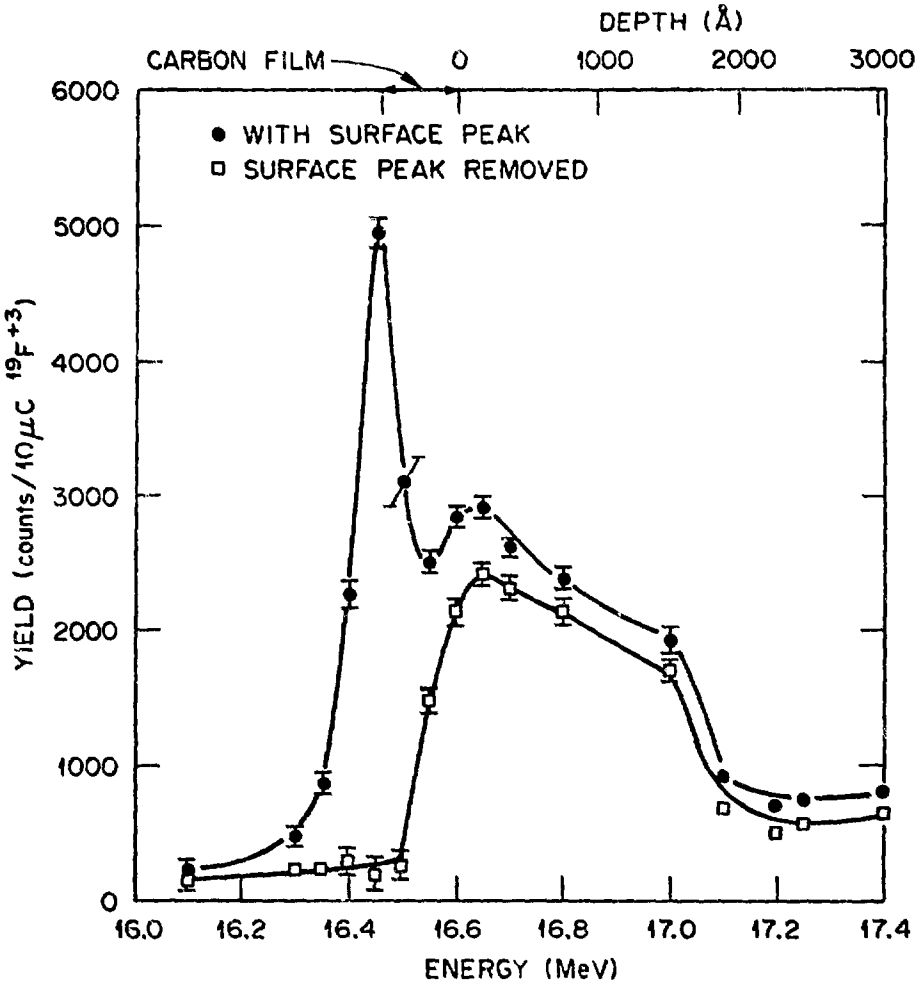

X_0 Synthetic Quartz : Hydrogen Profile.

Fig. 5

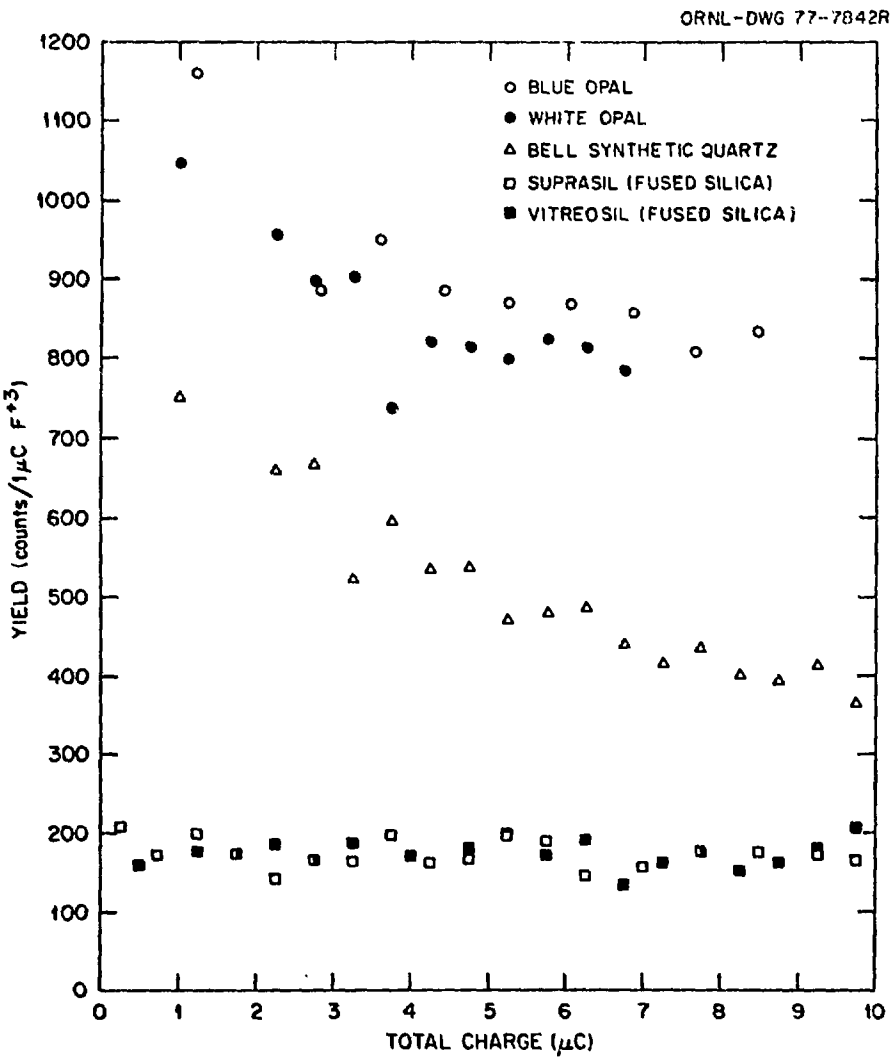

Apparent Hydrogen Concentration as Function of Integrated Charge.

Fig. 6

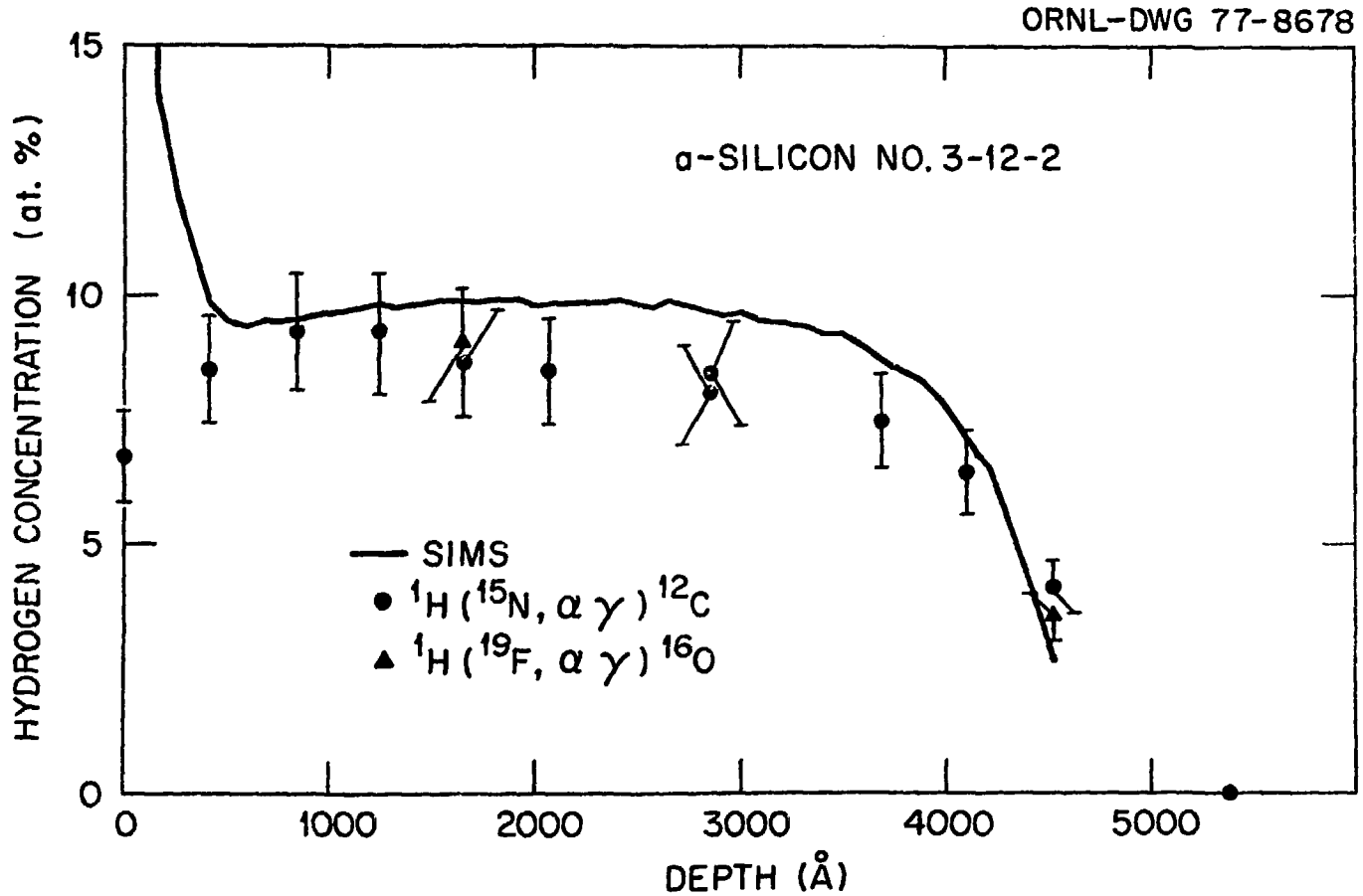
ORNL-DWG 77-8678
a-SILICON NO. 3-12-2
HYDROGEN CONCENTRATION (at. %)
DEPTH (Å)
SIMS
$^{1}H(^{15}N, \alpha\gamma)^{12}C$
$^{1}H(^{19}F, \alpha\gamma)^{16}O$
0
5
10
15
0
1000
2000
3000
4000
5000

Fig. 7